AIMS Geosciences

AIMS Geosciences, 12(2): 454–479.
DOI: 10.3934/geosci.2026017
Received: 23 January 2026
Revised: 16 February 2026
Accepted: 16 March 2026
Published: 15 April 2026

https://www.aimspress.com/journal/geosciences

Research article

Development of a flyrock prediction model for open-pit mining based on an analogy with the Navier-Stokes equations

Manuel Cánovas[1,*], Kevin Reyes[1], Raúl Meza[2], Elías Tapia[2], Javier Arzúa[1], Daniel Ibarra-González[1], Juan Francisco Sánchez-Pérez[3] and Emilio Trigueros[4]

[1] Metallurgical and Mining Engineering Department, Universidad Católica del Norte, Chile
[2] ENAEX, Chile
[3] Applied Physics and Naval Technology Department, Universidad Politécnica de Cartagena, Spain
[4] Mining and Civil Engineering Department, Universidad Politécnica de Cartagena, Spain

* **Correspondence:** Email: manuel.canovas@ucn.cl; Tel: +56967764324.

Abstract: Blasting is the most commonly used method for rock fragmentation in open-pit mining. Its objective is to achieve an adequate particle size for subsequent stages; however, not all the energy is utilized, and some energy is transformed into undesirable effects. Among these effects, flyrock is one of the most hazardous, as it endangers the safety of personnel, machinery, and infrastructure. Over the years, numerous flyrock prediction models have been developed based on different blasting and ground parameters. In the present study, a new predictive model is proposed for the maximum distance reached by a rock fragment based on the velocity obtained using an analogy with the Navier–Stokes equations. The development of the model considered three fundamental stages of fragment projection: (i) detonation of the explosive, which produces pressure on the blasthole perimeter owing to gas expansion, (ii) propagation of the kinetic energy transmitted through the rock mass until it reaches the propelled rock fragment, and (iii) trajectory of the flyrock. The resulting model depends on rock parameters (rock density), explosive parameters (density and energy of the explosive), design parameters (charge length, blasthole diameter, and burden), and a site-specific constant K, which can be determined using multiple regression analysis of the measured field data. A model consistency comparison was developed using Monte Carlo simulations, evaluating 100,000 realizations, demonstrating its potential for use. Similarly, a sensitivity analysis was performed, which verified that the burden was the parameter with the greatest influence within the model, whereas rock density had the least impact. Finally, as a future line of work, its application is proposed in ground conditions under different scenarios to strengthen its use in defining safety zones during blasting and to deepen the

physical understanding and meaning of parameter K, as its current interpretation still presents some degree of uncertainty.

Keywords: flyrock; blasting; Navier-Stokes equations; Monte Carlo simulation; open-pit

1. Introduction

Drilling and blasting operations are necessary in underground and open-pit mining. Explosives are also employed to excavate rock masses in civil construction works. Drilling and blasting are applied where mechanical means, such as bulldozers and hydraulic excavators, are unable to fragment the rock mass [1]. When an explosive charge detonates into a blasthole, gases at high temperature and pressure (on the order of a few GPa) are released [2]. Although blasting is the cheapest and fastest way to fragment hard rocks, only a reduced proportion of the detonation energy, approximately 20%–30%, is employed to fragment rocks [3–5]. The remaining energy is dissipated and is responsible for undesirable effects such as flyrocks, blast-induced ground vibrations, air overpressure, fumes, dust, and damage to rock mass [5–9].

Several similar definitions of flyrocks can be found in the scientific literature. The Institute of Makers of Explosives (IME) defines flyrock as the rock propelled beyond the blast area by the force of an explosion [10]. On the other hand, Raina et al. [11] defined flyrocks as the excessive random throwing of rock fragments from a blast that can travel distances beyond the desired values and present a serious threat to people and property in and around the mine. Finally, a more recent definition was provided by van der Walt and Spiteri [12], who defined flyrock as a rock fragment projected beyond the planned or expected throw distance, which is caused by the instantaneous release of explosive energy required to fracture a rock mass to the desired fragmentation and yield the desired muckpile profile. Flyrock can travel a distance greater than 600 m at velocities of up to 650 km/h [13,14].

According to Little [15], three types of flyrock can be recognized in bench blasting for open-pit mining: (i) burden throw, the blast-driven movement of broken rock to form the muck pile, which generally does not extend to more than ten bench heights and falls within the blast zone; (ii) normal flyrock, the propulsion of rock beyond the blast zone but falling within the exclusion zone; and (iii) wild flyrock, rock fragments propelled outside the clearance zone, often onto private and public areas. A particularly troublesome aspect of wild flyrock is that large fragments can reach unexpected distances from the blast site. There have been scattered reports of flyrock being thrown up to 1000 m [16]. Flyrock can result from three key mechanisms [17–20]: (i) face burst, which occurs when explosive charges intersect or are in close proximity to geological structures or zones of weakness; (ii) cratering, which takes place when the ratio of stemming height to blasthole diameter is too small or the collar rock is weak; and (iii) rifling, which occurs when stemming material is inefficient or absent.

As can be found in the scientific literature on blasting engineering, blast-induced ground vibrations or air overpressure have received much more attention from mining professionals and scholars than flyrock. Several countries have developed regulations to control these undesirable effects [11]. However, some authors consider flyrock to be the most hazardous of the undesirable effects related to blasting in open-pit mining. Flyrock represents a serious risk to people, machinery, and buildings within and outside the mining area [16,21–23]. Flyrock causes serious injuries at distances where blast-induced ground vibrations and air overpressure are insignificant [16].

The occurrence of flyrock is common in open-pit blasting. However, flyrock that does not cause injuries and/or infrastructure damage has not been reported. This is inconvenient because it could help improve the understanding of this phenomenon and the accuracy of predictive models [11]. According to some authors, flyrock is the main cause of many fatal and non-fatal accidents, more so than any other blasting-related accident [20,24]. Some authors have presented statistics on accident rates, in which flyrock was responsible for 24%–30% of the blasting-related accidents that occurred in open-pit mines [25–29].

Although significant efforts have been made in the last few decades to understand the generation of flyrock and predict the maximum distance reached, this phenomenon is less understood than blast-induced ground vibrations and air overpressure. To reduce flyrock and minimize its severe consequences, it is important to understand it [30].

As a result of blasting, flyrock occurrence and level of intensity are influenced by controllable and uncontrollable parameters. Controllable parameters are related to blasting design and can be modified (insufficient burden, improper delay time, inadequate stemming, inaccurate drilling, or non-adequate powder factor), whereas uncontrollable parameters are natural and cannot be changed (geological and geotechnical conditions or presence of water) [20,31].

Flyrock is caused by a mismatch in the distribution of explosive energy, type of confinement of the explosive charge, and mechanical strength of the rock. Factors responsible for this mismatch include [32] (i) abrupt change in the rock strength owing to the presence of joints, (ii) high explosive concentration leading to excessive localized energy density due to the migration of explosives into fissures or caverns, (iii) deviation of blastholes from the original design, causing a reduction of burden or spacing, (iv) insufficient or improper stemming leading to stemming ejection and bench-top flyrock, and (v) inappropriate or poor blast design.

Raina et al. [11] summarized the dominant reasons for flyrock occurrence as follows: (i) rock mass (inconsistent strata), (ii) blast design (burden, stemming, and delay), and (iii) execution (drilling and loading and face condition). The burden is considered the most relevant parameter for blasting design [33]. If the burden is below the optimal value, the gases generated by the detonation escape to the atmosphere, ejecting rock fragments in an uncontrolled manner. Otherwise, an excessive burden can cause flyrock because explosives are unable to fragment the burden rock volume; consequently, gases escape through the collar blasthole, generating a crater effect [34]. However, a spacing lower than the burden may generate crater effects and early stemming leakage among adjacent blastholes [17]. The blast delay sequence can also influence the generation of flyrock [35].

Ash [36,37] defined stiffness as the ratio of the bench height (H) to its burden (B). This ratio provides preliminary results for blasting. If the ratio H/B is greater than 3, appropriate fragmentation and no undesirable effects, such as blast-induced ground vibrations and flyrock, are expected. Most models developed in the last decades highlight burden, spacing, stemming, blasthole length, powder factor, and charge per delay as the most significant controllable parameters for flyrock generation [38].

Van der Walt and Spiteri [30] conducted a review of the approaches and techniques to predict flyrock, considering publications since 2010. The authors compiled key influential parameters for flyrock generation. As expected, the powder factor and stemming were key parameters. However, burden is not considered a critical parameter, which contradicts some publications and the face burst mechanism of flyrock. The authors stated that disregarding the importance of the burden supports the idea that the effect of blast parameters on flyrock is not fully known or understood.

To ensure the safety of people, machinery, and buildings within and outside mines, many models dealing with flyrock generation have been developed over the last few decades using different approaches and techniques. As the negative impacts of flyrock cannot be completely eliminated, only minimized, the models are a useful tool for determining safe areas for workers and machinery to be located. However, owing to the complexity of this phenomenon, there is a high degree of uncertainty in the results provided by these models. Some models require a large amount of data or are based on artificial intelligence (AI) approaches, which makes their application difficult. The main objective of this study is to develop a simple formula to estimate the maximum flyrock distance from the blasting parameters and the rock properties.

2. Flyrock models

The first models to predict maximum flyrock distance were developed by Lundborg [39] and Lundborg et al. [40]. Since these pioneering works, a large number of studies have been published that deal with models using different approaches. According to Raina et al. [11], these approaches can be classified as (i) mathematical models, (ii) empirical models, and (iii) fuzzy logic and artificial neural network-based models. A recent review of flyrock predictive models was conducted by van der Walt and Spiteri [30]. The authors considered four broad categories: (i) artificial intelligence (AI) [41–46], (ii) rock engineering systems [47,48], (iii) empirical and statistical analysis [49–51], and (iv) mechanistic or mathematical models, mainly based on ballistic analysis [40,52–56].

Traditionally, mechanistic and empirical models have been extensively used. Mechanistic models are based on the basic principles of physics and natural laws (Newton's three laws of motion) [53,57–58]. The advantage of these types of models is that they include universal mechanisms such as trajectory shape, air drag, or rock bounce, which are not site dependent. However, they require inputs such as launch angle, launch velocity, and fragment mass, which are difficult to obtain and may be site dependent [59].

Empirical and statistical analyses were the basis of the first models to predict the flyrock range [20,39,60–62]. These models do not explicitly consider physical mechanisms. Mathematical models were developed through statistical analysis, generally using multiple regression. The result is a simple equation for the flyrock range that involves a few variables considered to be the most significant, such as burden, rock density, stemming length, or charge per delay [35]. Some recent empirical and statistical models are based on dimensional analysis [20], multiple regression analysis and Monte Carlo simulations [63], or regression tree models [64]. The simplicity of empirical models is an advantage for their application. However, empirical correlations present several disadvantages [16]: (i) developed models are site-specific and cannot be applied as universal models under any blasting conditions; (ii) range predictions require a large amount of field data, including measured values of throw distance; (iii) equations do not provide any information on the size of rocks and its influence on the range; and (iv) empirical correlations do not identify the root causes of flyrock or the physical mechanisms responsible for flyrock projection.

Faramarzi et al. [47] developed a rock engineering system (RES)-based model to predict the flyrock distance and the corresponding risk in bench blasting. The RES concept was introduced by Hudson [65]. This methodology can simultaneously analyze the relationships between effective parameters. The interaction matrix is a basic method for representing relevant parameters and their interactions. The results demonstrated that the RES-based model is more precise than the multivariate regression analysis model (MVRM) and dimensional analysis (DA). However, the RES-

based model presented by Faramarzi et al. [47] is site-specific and cannot be generalized as a universal solution for all sites.

The more recent trend to predict flyrock is the use of AI approaches. AI prediction models deal with a measured set of flyrock ranges for given rock mass properties, explosive properties, and blast design parameters. This set is considered the input to the AI approach, which assigns weights to each of the contributing factors [35]. The output is highly dependent on the quality of the input parameters and the accuracy of the estimation of these parameters. AI algorithms have demonstrated to be effective in minimizing the uncertainties related to flyrock; however, there are still several uncertainties related to flyrock, as well as the blast parameters that directly influence the risk of flyrock and to what degree [30]. Some of the techniques that have been successfully applied are artificial neural networks (ANN) [41,58,66–68], adaptative neuro-fuzzy inference systems (ANFIS) [69–72], imperialist competitive algorithms (ICA) [73,74], support vector machines (SVM) [75–77], particle swarm optimizations (PSO) [78,79], genetic programming (GP) [80,81], gene expression programming (GEP) [82–84], ant colony optimizations (ACO) [85–87], firefly algorithm (FA) [88–90], and Harris hawk optimizations (HHO) [91–92], among others.

Table 1 summarizes some of the most commonly used equations to estimate the maximum distance and initial velocity reached by the fragments. Later, these equations will be employed for comparison with the mathematical model developed in the present study.

Table 1 Predictions equations for flyrock.

Model	Equation
Lundborg et al. [40]	$L_{max} = 260 \cdot d^{2/3}$
Roth [61]	$V_0 = (2E)^{0.5} \cdot q_l / m_l$
Bagchi and Gupta [62]	$L_{max} = \left(\frac{T}{155.2 \cdot B}\right)^{-0.73}$
Richard and Moore [52]	$L_{max} = \frac{k^2}{g}\left(\frac{\sqrt{m}}{B}\right)^{2.6}$ (*face burst*)
	$L_{max} = \frac{k^2}{g}\left(\frac{\sqrt{m}}{T}\right)^{2.6}$ (*cratering*)
	$L_{max} = \frac{k^2}{g}\left(\frac{\sqrt{m}}{T}\right)^{2.6} \cdot \sin 2\theta_0$ (*rifling*)
McKenzie [93]	$L_{max} = 11 \cdot SDOB^{-2.167}\left(\frac{d}{F_s}\right)^{0.667}$
Trivedi et al. [94]	$L_{max} = \frac{10^{5.1} \cdot q_l^{0.51} \cdot q^{0.14}}{B^{0.93} \cdot T^{0.64} \cdot \sigma_c^{0.75} \cdot RQD^{0.93}}$

where L_{max}: flyrock range; d: blasthole diameter; V_0: flyrock initial velocity; E: Gurney constant; q_l: lineal charge concentration of explosive; m_l: mass per length unit; T: stemming; B: burden; k: constant; g: gravity acceleration; m: lineal charge density; θ: blasthole angle; $SDOB$: scale depth of burial; Fs: shape factor; q: powder factor; σ_c: uniaxial compressive strength of the rock; and RQD: rock quality design.

From the prediction models, some authors have defined criteria to delimit danger and safety zones in blasting based on probabilistic methods [95,96]. Raina et al. [97] established that the maximum projection distance cannot overcome half the distance where personnel and equipment are protected.

For small-scale blasting, evacuation zones between 100 and 300 m must be applied, whereas for larger-scale blasting, more than 500 m are usually employed. However, the different conditions of each blasting must be considered, especially when multiple charges, non-coupled cartridges, or air-decks are used. According to Chernigovskiĭ [98], it is not possible to calculate projection trajectories with a precision greater than 20% because air resistance and initial velocity are unknown variables. Therefore, the application of a Factor of Safety (FoS) is recommended, as suggested by McKenzie [93].

3. Mathematical model

The proposed model is developed in three fundamental stages that allow the determination of the maximum projection distance of a rock fragment: (i) detonation of the explosive charged into a blasthole, (ii) energy propagation through the surrounding rock mass until the considered rock fragment, and (iii) trajectory of the flyrock to define the maximum distance reached.

For the initial approach to the problem, the momentum equation of the Navier–Stokes equations is employed (Equation 1). The Navier–Stokes equations describe the motion of viscous fluids. The proposed model is based on an analogy between the motion of viscous fluids and blasting energy propagation through rock masses using the momentum transfer equation of the Navier–Stokes equations. This hypothesis considers a series of simplifications. The most important aspect is the transition from fluid dynamics to rock mechanics by comparing the motion of viscous fluids with blasting energy propagation, which occurs in discontinuous, anisotropic, and damage-susceptible solid rock masses [99–101]. The validation of this simplification is discussed in the Results and Discussion section by comparing the results of the proposed model with those of the models collected from the state-of-the-art review.

$$\rho \frac{D\vec{v}}{Dt} = -\nabla P + \rho \vec{g} + \mu \nabla^2 \vec{v} \tag{1}$$

By introducing the total derivative term, Equation 1 becomes:

$$\rho \left[\frac{\partial \vec{v}}{\partial t} + (\vec{v} \cdot \nabla)\vec{v} \right] = -\nabla P + \rho \vec{g} + \mu \nabla^2 \vec{v} \tag{2}$$

$$\frac{\partial \vec{v}}{\partial t} + (\vec{v} \cdot \nabla)\vec{v} = -\frac{1}{\rho}\nabla P + \vec{g} + \frac{\mu}{\rho}\nabla^2 \vec{v} \tag{3}$$

Being $\vec{v}$ the velocity vector (m/s), ρ the fluid density (g/cm^3), P the pressure (Pa), μ the dynamic viscosity of the fluid (N·s/m^2), and g the gravitational acceleration (m/s^2).

Because the forces propagate in a solid medium instead of a fluid, some hypotheses must be established. For this case, an incompressible ($\nabla \vec{v} = 0$) and irrotational fluid ($\nabla^2 \vec{v} = 0$) is assumed to simulate the characteristics of a continuous rock mass so that the advective and viscosity terms can be eliminated. Thus, terms of Eq. 3 can be regrouped as follows:

$$\frac{\partial \vec{v}}{\partial t} + \frac{1}{\rho}\nabla P - \vec{g} = 0 \tag{4}$$

As the vectorial field of velocities can be considered as a conservative field, a potential function is defined:

$$\vec{v} = -\nabla\Phi \tag{5}$$

Working in terms of the potential function of the vectorial field of velocities, Eq. 6 is obtained:

$$\frac{\partial(-\nabla\Phi)}{\partial t} + \frac{1}{\rho}\nabla P - \vec{g} = 0 \tag{6}$$

By factoring the nabla operator and solving the resulting integral, Eqs. 7 and 8 are obtained, where z is the height (m), and C is a constant (m^2/s^2) from the integral.

$$\nabla\left(\frac{-\partial\Phi}{\partial t} + \frac{P}{\rho} - (-\vec{g}z)\right) = 0 \tag{7}$$

$$-\frac{\partial\Phi}{\partial t} + \frac{P}{\rho} + \vec{g}z = C \tag{8}$$

The pressure generated by the explosive detonation is much larger than the influence of the gravitational field; therefore, the last term can be neglected:

$$\frac{P_w}{\rho_r} \gg \vec{g}z \tag{9}$$

Where P_w is the exercised pressure on the surrounding media immediately after the blasthole walls (Pa), and ρ_r is the rock density (g/cm^3). Thus, Eq. 8 is simplified as follows:

$$\frac{\partial\Phi}{\partial t} = \frac{P_w}{\rho_r} \tag{10}$$

The potential function must be solved to determine the initial velocity of the rock fragment. The introduction of the potential function represents an equivalent scalar energy field that describes the radial transfer of explosive energy under the simplified assumptions of spherical symmetry and irrotational propagation. In this context, the results obtained are consistent with those reported in the literature for the face burst mechanism.

$$\Phi = \int \frac{P_w}{\rho_r} dt \tag{11}$$

An expression for Φ as a function of the distance parameters is required. To obtain this expression, the following equations for the pressure levels generated by the detonation of an explosive are used [102]:

$$P_d = \frac{\rho_{exp} \cdot VOD^2}{4} \tag{12}$$

$$P_e = \frac{P_d}{2} = \frac{\rho_{exp} \cdot VOD^2}{8} \tag{13}$$

$$P_w = P_e \left(\frac{V_e - \alpha_e}{V_h - \alpha_h}\right) \tag{14}$$

Where P_d is the detonation pressure of the explosive (MPa), P_e is the exercised pressure on blasthole walls for coupled charges (MPa), P_w is the exercised pressure on blasthole walls for non-coupled charges considering non-ideal gases (MPa), *VOD* is the explosive velocity of detonation (m/s), ρ_{exp} is the explosive density (g/cm^3), V_e is the explosive volume (m^3), and V_h is the gas volume filling the blasthole (m^3). Finally, αe and αh are volumetric correction coefficients that are calculated by means of Eqs. 15 and 16:

$$\alpha_e = 1.1 \cdot e^{-0.473 \cdot V_e} \tag{15}$$

$$\alpha_h = 1.1 \cdot e^{-0.473 \cdot V_h} \tag{16}$$

The force applied by the explosive gases generated during detonation can be obtained based on a two-dimensional analysis of the pressure on the surrounding rock mass, as shown in Figure 1.

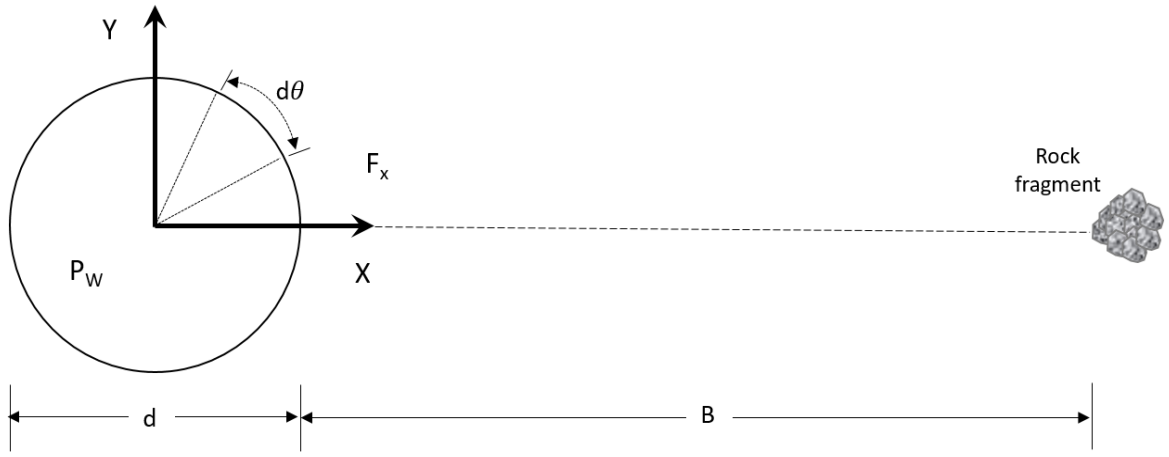

Figure 1. Two-dimensional analysis of the distribution of forces resulting from pressure P_w.

The pressure on the blasthole walls can be expressed as the ratio of a force differential to a cylinder surface differential, considering a 1-m depth cylinder; it must be considered as an implicit unit in the equation, which corresponds to a portion of the circumference perimeter shown in Figure 1. The pressure P_w can be expressed as follows:

$$P_w = \frac{dF_i}{r_h \cdot d\theta} \tag{17}$$

Operating with the force differential and considering its contributions on the abscissa axis, Eqs. 18–21 are obtained. Note that only the right half of the circumference is considered to determine the force at which the rock fragment is projected.

$$dF_i = r_h \cdot P_w \cdot d\theta \tag{18}$$

$$F_x = \int_{-\pi/2}^{\pi/2} r_h \cdot P_w \cdot \cos\theta \cdot d\theta \tag{19}$$

$$F_x = r_h \cdot P_w \int_{-\pi/2}^{\pi/2} \cdot \cos\theta \cdot d\theta \tag{20}$$

$$F_x = 2 \cdot r_h \cdot P_w \tag{21}$$

Where F_x is the force exerted by the explosive detonation, r_h is the blasthole radius, and P_w is the pressure exerted on the blasthole walls. Previously, the potential function of the velocity field was defined in Eq. 11. This function depends on the pressure developed by the explosive detonation; thus, P_w must be determined.

$$P_w = \frac{F_x}{2 \cdot r_h} \tag{22}$$

The pressure P_w can be replaced to express the potential function Φ of the velocity field as a function of the force F_x:

$$\Phi = \int \frac{F_x}{2 \cdot r_h \cdot \rho_r} dt \tag{23}$$

Operating F_x as a function of time, the expression for linear momentum p is obtained as follows:

$$\Phi = \frac{p}{2 \cdot r_h \cdot \rho_r} \tag{24}$$

On the other hand, the projection velocity of the rock fragment can be obtained from the kinetic energy, E_k, which is quantified per unit volume using the following equations:

$$E_k = \frac{1}{2} \cdot m \cdot v^2 \tag{25}$$

$$\frac{dE_k}{dV} = \frac{d}{dV}\left(\frac{1}{2} \cdot m \cdot v^2\right) \tag{26}$$

$$dE_k = \frac{\rho_r}{2} \cdot v^2 \cdot d \tag{27}$$

Where E_k is the kinetic energy (kJ), ρr is the rock density (kg/m^3), v is the projection velocity (m/s), and dV is the volume differential (m^3). By solving the integral and replacing the potential function instead of the projection velocity, Eqs. 28–29 are obtained:

$$E_k = \frac{\rho_r}{2} \cdot \iiint v^2 \cdot dV \tag{28}$$

$$E_k = \frac{\rho_r}{2} \cdot \iiint (\nabla \Phi)^2 \cdot dV \tag{29}$$

Rewriting Eq. 29 and using the Green theorem for a harmonic function, the following expressions are obtained:

$$E_k = \frac{\rho_r}{2} \cdot \iiint (\nabla \Phi) \cdot (\nabla \Phi) \cdot dV \tag{30}$$

$$E_k = \frac{\rho_r}{2} \cdot \oiint \Phi \cdot \frac{\partial \Phi}{\partial \mathrm{n}} \cdot dS \tag{31}$$

As the medium is assumed to be incompressible, the energy does not depend on the shape of the surface containing the explosive charge but depends on the distance between the detonation focus and the study point. Thus, the expression can be rewritten in terms of the distance *r*.

$$\frac{\partial \Phi}{\partial n} = \frac{\partial \Phi}{\partial r} \tag{32}$$

$$E_k = \frac{\rho_r}{2} \cdot \Phi \oiint \frac{\partial \Phi}{\partial \mathrm{r}} \cdot dS \tag{33}$$

Eq. 24 can be introduced into Eq. 33 to obtain the following equations:

$$E_k = \frac{\rho_r}{2} \cdot \left(\frac{p}{2 \cdot r_h \cdot \rho_r}\right) \oiint \frac{\partial}{\partial \mathrm{r}}\left(\frac{p}{2 \cdot r_h \cdot \rho_r}\right) \cdot dS \tag{34}$$

$$E_k = \left(\frac{p}{4 \cdot r_h}\right) \oiint \left(\frac{p}{r_h^2 \cdot \rho_r}\right) \cdot dS \tag{35}$$

$$E_k = \left(\frac{p^2}{4 \cdot r_h^3 \cdot \rho_r}\right) \oiint \cdot dS \tag{36}$$

If the energy generated by spherical charges is considered, the surface *dS* is equivalent to a sphere; hence, the following expression for the kinetic energy is deduced:

$$E_k = \left(\frac{p^2}{4 \cdot r_h^3 \cdot \rho_r}\right) \cdot 4\pi \cdot r_h^2 \tag{37}$$

$$E_k = \frac{p^2 \cdot \pi}{r_h \cdot \rho_r} \tag{38}$$

Assuming that the total energy from the explosive charged into the blasthole, E_{total}, is transferred as kinetic energy ($E_{total} = E_{kinetic}$), the following approximation to solve p (linear momentum) can be obtained:

$$p = \sqrt{\frac{E_{total} \cdot \rho_r \cdot r_h}{\pi}} \tag{39}$$

Using this expression, the potential function of the velocity field can be calculated as follows:

$$\Phi = \frac{1}{2 \cdot r \cdot \rho_r} \sqrt{\frac{E_{total} \cdot \rho_r \cdot r_h}{\pi}} \tag{40}$$

Considering that the velocity vector is equal to the gradient of the potential function ($\vec{v} = -\nabla\Phi$), the flyrock velocity at a distance "*r*" from the detonation point can be determined using the following equations:

$$\vec{v} = -\nabla\left(\frac{\mathrm{p}}{2 \cdot r \cdot \rho_r}\right) \tag{41}$$

$$\vec{v} = -\frac{\partial}{\partial \mathrm{r}}\left(\frac{\mathrm{p}}{2 \cdot r \cdot \rho_r}\right) \tag{42}$$

$$\vec{v} = -\frac{\partial}{\partial \mathrm{r}}\left(\frac{\mathrm{p}}{2 \cdot r \cdot \rho_r}\right)\sqrt{\frac{E_{total} \cdot \rho_r \cdot r_h}{\pi}} \tag{43}$$

Finally, the expression for the flyrock initial velocity is a function of the square of the distance between the detonation focus and the flyrock, total energy of the explosive, blasthole radius, and rock density.

$$v_0 = \frac{1}{\mathrm{r}^2}\sqrt{\frac{E_{total} \cdot r_h}{\pi \cdot \rho_r}} \tag{44}$$

The formulation of Eq. 44 provides the results for intact rock. However, a correction coefficient obtained from field tests must be added to obtain a more realistic estimation. So, Eq. 44 can be rewritten as a function of the correction coefficient *K* and the effective burden as the distance *r*.

$$v_0 = K \cdot \frac{1}{\mathrm{B}^2}\sqrt{\frac{E_{total} \cdot r_h}{\pi \cdot \rho_r}} \tag{45}$$

The next step is to calculate the maximum flyrock distance. By applying the equations of the parabolic trajectory of bodies in free fall, the maximum flyrock distance can be estimated by considering the bench height.

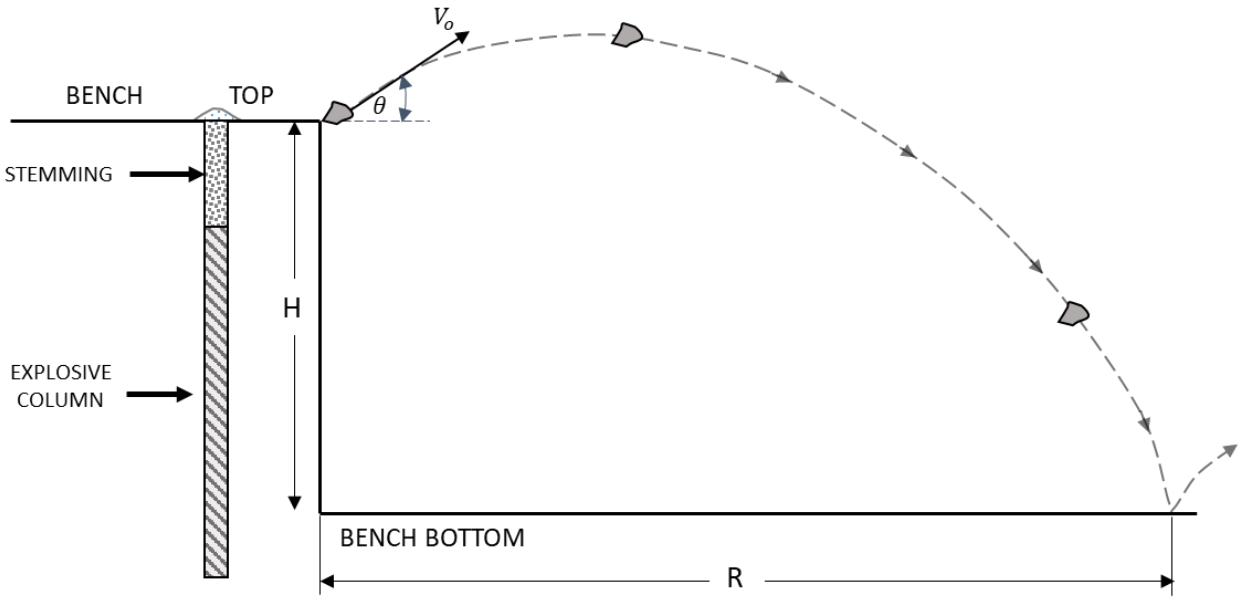

Figure 2. Scheme of maximum flyrock distance considering a height (modified from Chiapetta and Mammele [103]).

$$R = (v_0 \cdot \cos\theta)\frac{(v_0 \cdot \sin\theta) + \sqrt{(v_0 \cdot \sin\theta)^2 + 2 \cdot g \cdot H}}{g} \quad (46)$$

Where R is the maximum flyrock distance considering the bench height, v_0 is the initial flyrock velocity, H is the initial projection height, and θ is the angle between the velocity vector (tangent) and the horizontal axis (Figure 2).

Through Eqs. 45 and 46, a quadratic fit analysis can be performed to determine the correlation between the maximum distance and the initial velocity, resulting in Eq. 47. The analysis was carried out considering a 45° angle and a 10-m initial height to obtain a more conservative result for security issues.

$$L_{max} = C \cdot v_0^{\alpha} + \varepsilon \quad (47)$$

Where L_{max} is the maximum flyrock distance, C is a constant, α is the exponential coefficient, and ε is the error. For velocities equal to or greater than 12 m/s and lower than 180 m/s, α and C are approximately 2 and 0.102 s^2/m, respectively, and L_{max} presents an average error of ± 9 m (Eq. 48). Later, using Eq. 45, Eq. 48 can be rewritten as follows:

$$L_{max} = 0.102 \cdot v_0^2 + 9 \quad (48)$$

$$L_{max} = 0.102 \cdot \left(K \cdot \frac{1}{\mathrm{B}^2} \sqrt{\frac{E_{total} \cdot r_h}{\pi \cdot \rho_r}} \right)^2 + 9 \quad (49)$$

$$L_{max} = K^2 \frac{0.102 \cdot E_{total} \cdot r_h}{\mathrm{B}^4 \cdot \pi \cdot \rho_r} + 9 \quad (50)$$

A previous calculation is still required to obtain the total energy (kJ), which can be obtained by considering the explosive energy per kilogram (kJ/kg) and the total amount of explosive charged into the blasthole.

$$E_{total} = E_{exp} \cdot \rho_{exp} \cdot \left(\pi \cdot \left(\frac{d}{2} \right)^2 \cdot L_c \right) \cdot 10^3 \quad (51)$$

Where E_{total} is the total energy of the explosive charged into the blasthole (kJ), E_{exp} is the explosive energy (kJ/kg), ρ_{exp} is the explosive density (g/cm^3), d is the blasthole diameter (m), and L_c is the explosive charge length (m). Finally, two equations are proposed to obtain the maximum flyrock distance. Eq. 52 can be used if the total amount of explosive charge into the blasthole is known (Q). On the other hand, Eq. 53 is obtained by combining Eqs. 50 and 51.

$$L_{max} = K^2 \frac{0.102 \cdot E_{exp} \cdot Q \cdot d}{2 \cdot \mathrm{B}^4 \cdot \pi \cdot \rho_r} + 9 \quad (52)$$

$$L_{max} = K^2 \frac{12.75 \cdot E_{exp} \cdot \rho_{exp} \cdot L_c \cdot d^3}{B^4 \cdot \rho_r} + 9 \quad (53)$$

Although the model provides an explicit formula for the maximum projection distance of fragments under the indicated application conditions, Eq. 54, a simplified expression for the initial velocity is also presented, being obtained from Eq. 45 and 51. This simplified formula can be directly coupled with the parabolic trajectory equation (Eq. 46) to estimate the flyrock reach. Nevertheless, aerodynamic effects may become more relevant at higher velocities, and their incorporation represents a natural extension of the proposed analytical framework.

$$v_o = \frac{K}{2}\left(\frac{E_{exp}}{2} \cdot 10^3\right)^{0.5} \left(\frac{\rho_{exp}}{\rho_r}\right)^{0.5} \left(\frac{L_c}{B}\right)^{0.5} \left(\frac{d}{B}\right)^{1.5} \quad (54)$$

Moreover, the proposed equation is not limited to the adopted ballistic formulation and can be integrated into other models; for example, those that incorporate aerodynamic effects, such as air resistance. Finally, it should be noted that the *K* parameter ranges approximately from 14 to 29 when initial velocities between 26 and 42 m/s are assumed, considering the typical range of variability for the other parameters involved. This range provides a consistent calibration interval for the proposed model and supports its applicability under realistic blasting conditions.

4. Results and discussion

The proposed model aims to explain the propagation of the kinetic energy that drives and projects rock fragments, using physical and hydrodynamic principles. Recognizing that this propagation occurs through the rock mass, which is a discontinuous, anisotropic, and heterogeneous medium, the formulation considers a series of physical simplifications intended to represent the phenomenon without exhaustively describing its complexity.

The use of the constant K is not new in flyrock prediction models, as it was introduced by Richard and Moore (2004) [52], where it is considered a constant. A clear analogy can be established between the K factor of the developed model and the K factor of the PPV vibration prediction models (general law of the blasting vibration attenuation equation), and it deserves to be studied in detail. K is a site-specific constant that represents the influence of (i) blast design and detonation propagation, (ii) physical properties of the transmitting medium, that is, local geology, and (iii) site topography. K can be determined using multiple regression analysis of the measured field data [1]. In the developed model, K also considers air-related factors such as air resistance or wind velocity, and rock fragment size, shape, and weight.

To compare the proposed model, different predictive formulas were preliminarily evaluated under the same mechanical conditions and design characteristics. The values used for this comparison are listed in Table 2. It should be noted that the evaluated values serve only an illustrative purpose, with average values calculated from publications; thus, they may not reflect the actual conditions of a mining operation, and the results should be interpreted within this context.

Table 2. Parameters used for model comparison.

Parameters	Description	Value	Unit
ρ_r	Rock density	2.7	t/m^3
ρ_{exp}	Explosive density	1.3	t/m^3
E_{exp}	Explosive energy	3247	kJ/kg
VOD	Velocity of detonation	4250	m/s
d	Diameter	0.3175	m
L_c	Large of explosive column	7	m
T	Stemming	3	m
B	Burden	9.23	m
F_s	Shape factor	1.3	-
q	Powder factor	0.36	kg/t
q_l	Lineal charge	0.671	kg/m
m_l	Mass per length	720.47	kg/m
RQD	Rock quality design	40	%
σ_c	Uniaxial compressive strength	120	MPa

The results obtained by each model considering a launch angle of 45° are listed in Table 3. The maximum projection distance according to the Roth model [61] was determined by solving for the initial velocity using the following launch equation. For the Richard and Moore model [52], a constant $K=27$ was used, while for the proposed model, a constant $K=18$ was used.

Based on the results, it can be observed that the Lundborg model predicts a higher maximum projection distance, whereas the Trivedi et al. model predicts the lowest maximum distance. The proposed model predicted a maximum reach of 208.58 m. This remains within the broader range reported by the models considered, indicating that the proposed formulation provides a consistent order of magnitude for the maximum flyrock reach. The explicit forms of Eqs. (52) and (53) allow their direct practical implementation using blasting design parameters without the need for iterative procedures.

Table 3. Comparison of the maximum projection distance by model.

Models	Parameters	Maximum distance (m)
Lundborg et al. [40]	d, ρ_r	1400
Roth [61]	*VOD*, q_l, m_l	317
Bagchi and Gupta [62]	B, T	90
Richard and Moore [52]	B, q_l, K	95
McKenzie [93]	D, F_s, *SDOB*	1025
Trivedi et al. [94]	B, T, q_l, q, *RQD*, *UCS*	64.91
Proposed model	E_{exp}, ρ_r, ρ_{exp}, L_c, B, d	209

Subsequently, to understand the kinematic behavior of the flyrock, a set of representative trajectories obtained under different launch conditions was generated. The analysis considered three launch angles (30°, 45°, and 60°) and three initial launch heights (5, 10, and 15 m) and observed their effects on the trajectories and maximum fragment reach (Figure 3).

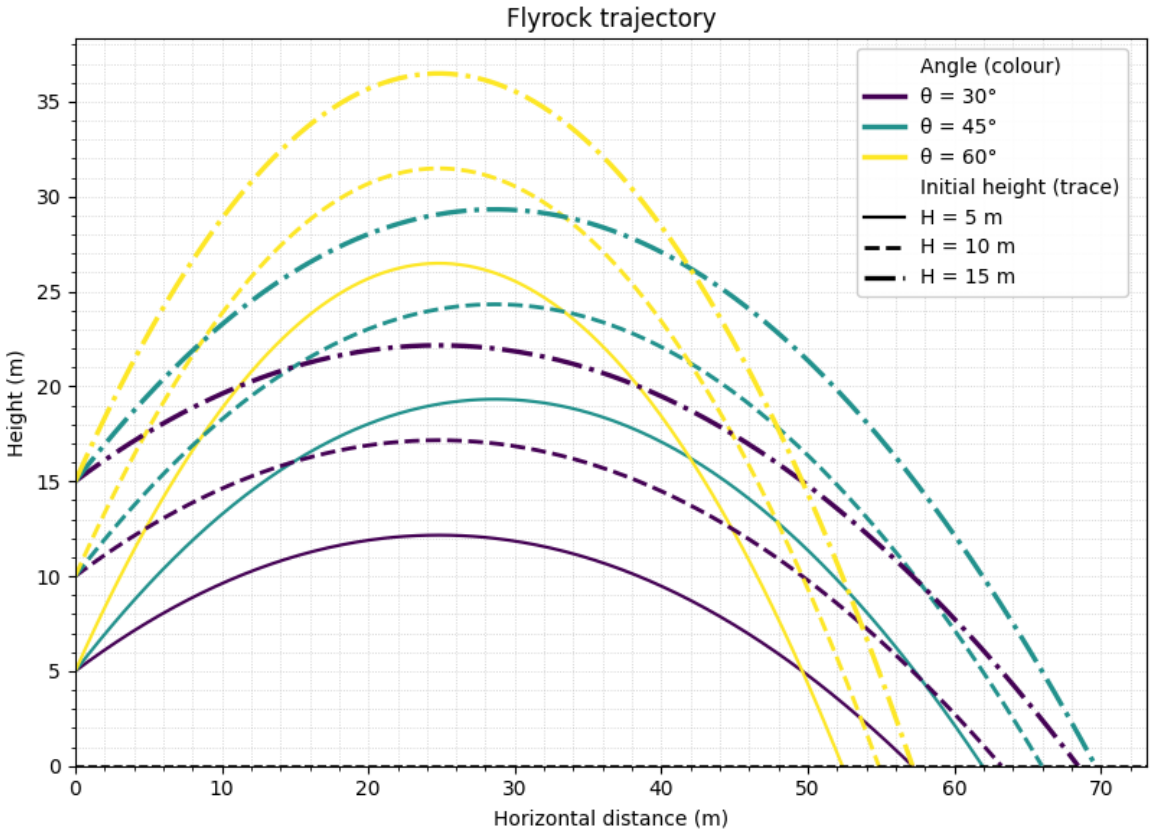

Figure 3. Maximum projection distance considering launch angles of 30°, 45°, and 60° and heights of 5, 10, and 15 m.

As stated in the Introduction, only a reduced proportion of the detonation energy is employed to fragment the rock mass; however, the model was developed assuming that the total explosive energy is entirely converted into the kinetic energy of the flyrock. This assumption can be solved by introducing an energy conversion efficiency that can be obtained using actual blast data. However, considering that the total explosive energy is entirely converted into the kinetic energy of the flyrock provides more conservative results, which are normally used to define safety zones due to flyrock in mining operations. On the other hand, as shown in Equation (37), the model was developed assuming spherical charges, that is, spherical symmetric energy propagation; however, it could be less realistic because actual blasting typically involves columnar charges. This assumption is an equivalent spherical source approximation that can be calibrated using actual blast data.

4.1. Monte Carlo simulation

To evaluate different possible scenarios associated with the variation of model parameters, simulations were carried out using the Monte Carlo method under different blasting design conditions and rock characteristics. Therefore, the input parameters were represented by probabilistic distributions by selecting the appropriate type of distribution and range and assigning representative values (Table 4).

A total of 100,000 realizations were performed, assuming independence between the input parameters; therefore, any interaction or correlation effects between them were not considered. This

assumption was adopted as a simplifying hypothesis to isolate the individual contributions of each parameter and facilitate the interpretation of uncertainty propagation within the model. However, in practical blasting design, parameters such as burden (B), charge length (L_c), and blasthole diameter (d) may exhibit operational or geometric correlations. Neglecting such dependencies may influence the probability distribution of the output variable and slightly affect the scenario dispersion. Future research should incorporate correlated input variables based on field data to enhance the realism of this probabilistic framework. In addition, the bench height and launch angle were maintained constant at 10 m and 45°, respectively, to focus the probabilistic analysis on the variability of the design and rock parameters rather than the geometric trajectory effects.

Table 4. Input parameters for Monte Carlo simulations.

Parameter	Unit	Type of distribution	Minimum value	Mean value	Maximum
K	-	Triangular	15	17	18
E_{exp}	kJ/kg	Uniform	630	-	885
ρ_{rock}	t/m^3	Triangular	2.4	2.7	2.8
ρ_{exp}	t/m^3	Triangular	1	1.2	1.3
L_c	m	Triangular	5	6	7
B	m	Triangular	4	5	6
d	mm	Uniform	152	-	165

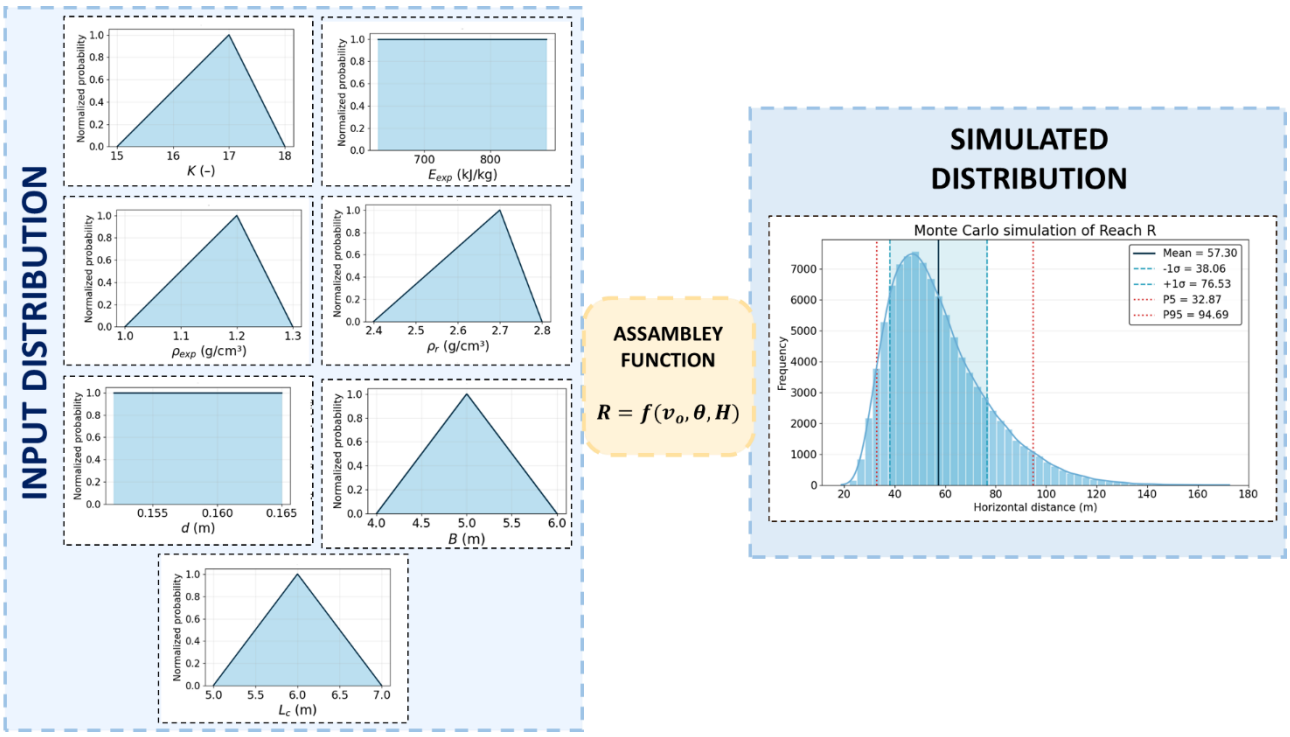

Figure 4. Monte Carlo simulation considering input distribution, assembly function, and simulated distribution.

Figure 4 shows the probability distributions of the input parameters considered in the Monte Carlo simulation, along with the resulting distribution of the output variable R (maximum flyrock reach)

during the simulation process. The input parameters were modeled using independent probability distributions according to the ranges and shapes defined in Table 4.

From the 100,000 realizations, the simulated distribution of R exhibited an asymmetric behavior, with a long tail toward higher values, reflecting the effect of the uncertainty of the input parameters on the response variable. Additionally, it can be observed that the mean value is 57.30 m, while the P_5 and P_{95} percentiles indicate a probable range of variation between 38.06 and 94.69 m, respectively.

The results show that under the evaluated design conditions, the model's response presents considerable dispersion, which is associated with the large ranges of the assessed input parameters. Similarly, the shape of the distribution suggests that scenarios with greater reach, although less probable, cannot be disregarded and should be considered in risk assessments and when defining the safety zone.

4.2. Spearman correlation analysis

To better understand the origin of the variability and identify the parameters that determine the observed dispersion in the results, a sensitivity analysis based on the Spearman correlation coefficient was performed. This analysis makes it possible to identify the relative influence of each input parameter, allowing the capture of nonlinear monotonic relationships, making it suitable for the nature of the evaluated models. It should be noted that the analysis was conducted under the assumption of statistical independence among the input variables, which is consistent with the adopted Monte Carlo approach. This assumption facilitates the interpretation of individual parameter effects; potential correlations among blasting design variables in real scenarios may alter the relative influence of certain parameters.

Figure 5 shows the sensitivity analysis of the fragment range (R). The results indicated that burden (B) was the parameter with the greatest influence, exhibiting a strong negative correlation with the output variable ($r_s = -0.89$). This confirms that the geometry, particularly the level of charge confinement, governs the kinematic response of the fragment. In contrast, explosive energy (E_{exp}) showed a moderate positive correlation, indicating that higher explosive energy increases the initial velocity and, therefore, the range of the fragment ($r_s = 0.25$). Similarly, the K coefficient, blasthole diameter (d), and charge length (L_c) exhibited a lower and similar positive influence ($r_s = 0.18–0.19$).

The strong negative correlation observed for burden (B) can be physically interpreted in terms of charge confinement and energy transmission efficiency. A smaller burden implies reduced confinement of explosive energy, facilitating higher fragmentation acceleration and, consequently, greater initial velocities and reach. However, an increasing burden enhances confinement and energy dissipation within the rock mass, thereby reducing the kinetic energy of the fragment projection. Moreover, according to Eq. (54), the initial velocity v_0 is inversely proportional to B^2, and this inverse dependence mathematically explains why the burden emerges as the dominant parameter in the sensitivity analysis. Furthermore, the multiplicative structure of the velocity equation implies that geometric parameters embedded in power-law relationships tend to amplify their influence on the output variability.

It should be noted that previous studies, such as the review conducted by van der Walt and Spiteri [30], identified the powder factor and stemming length as dominant parameters without highlighting the burden as critical. While stemming length can play a fundamental role in mechanisms where loss of confinement occurs owing to collar failure or cratering, the present formulation specifically addresses the face burst mechanism, in which the burden directly governs the confinement and energy transmission toward the free face.

Finally, explosive density (ρ_{exp}) had a weak positive influence, whereas rock density (ρ_r) was negatively correlated ($r_s = -0.08$), suggesting that it plays a lesser role than the design parameters. From the overall analysis, it can be concluded that the fragment range is primarily controlled by geometric factors rather than explosive or rock properties. In this sense, the analysis identifies the critical parameters that should be prioritized during the flyrock risk assessment phase, as well as in probabilistic analyses aimed at achieving this objective.

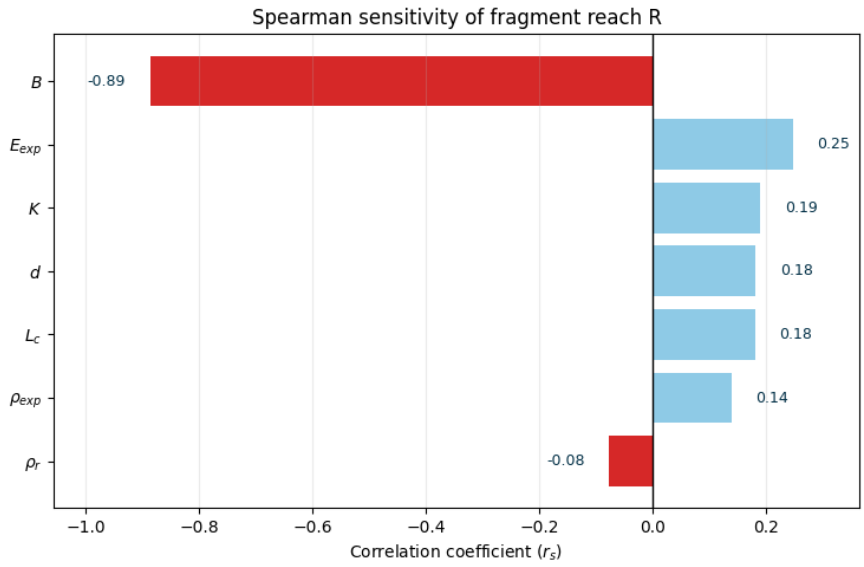

Figure 5. Spearman sensitivity analysis for the proposed model.

5. Conclusions

The operational pace of modern mining operations requires simple and efficient methods for estimating the safety zones associated with blasting. The use of advanced modeling and simulation techniques can provide more accurate estimates of the maximum distances reached by rock fragments; however, their application depends on the availability of extensive, site-specific databases. In contrast, empirical flyrock models, while lacking high precision, are known for their simplicity and speed of application.

In this study, a predictive model with easy application was developed to estimate the maximum projection distance of a rock fragment generated during a blast. The model is based on an analogy between the motion of viscous fluids and blasting energy propagation through rock masses using the momentum transfer equation of the Navier–Stokes equations, which represents this phenomenon in a simplified manner. The results obtained were similar to those obtained using equations from other authors, demonstrating the consistency of the proposed approach for the face burst mechanism. Therefore, the simplification developed by comparing viscous fluids with rock masses can be considered consistent.

To evaluate the influence of input parameter variability, a simulation was performed using the Monte Carlo method under different blasting and rock conditions. The results showed significant dispersion in the maximum projection distances, reflecting the uncertain nature of this phenomenon in the study. Additionally, a sensitivity analysis was conducted, demonstrating that the maximum

distance predicted by the model was determined mainly by burden, whereas the other parameters contributed secondarily.

It should be noted that the model has not yet been validated through field tests; therefore, the results obtained should be used with caution, especially if they are used directly to define safety zones in mining operations. The next step is to test the model with actual blast data from different open-pit mines to demonstrate its practical accuracy and reliability. Another important issue is improving the understanding of the site-specific constant K by incorporating physical effects such as air resistance, wind velocity, and rock fragment size, shape, and weight.

Author contributions

Conceptualization, M.C., K.R., R.M. and E.T.; methodology, M.C., K.R., R.M., E.T., J.A. and D.I.-G.; simulation, M.C., K.R., D.I-G., J.F.S.-P. and E.T.; validation, J.F.S.-P. and E.T.; formal analysis, J.A., J.F.S.-P. and E.T.; data curation, M.C. and D.I-G.; writing—original draft preparation, M.C., J.A., R.M., J.F.S.-P. and E.T.; writing—review and editing, .M.C., K.R., J.A., R.M., J.F.S.-P. and E.T.. All authors have read and agreed to the published version of the manuscript.

Use of AI tools declaration

The authors declare they have not used Artificial Intelligence (AI) tools in the creation of this article.

Acknowledgments

The authors acknowledge ENAEX for the support of this work.

Conflict of interest

The authors declare they have not conflict of interests

References

1. Trigueros E, Cánovas M, Muñoz JM, et al. (2017) A methodology based on geomechanical and geophysical techniques to avoid ornamental stone damage caused by blast-induced ground vibrations. *Int J Rock Mech Min Sci* 93: 196–200. https://doi.org/10.1016/j.ijrmms.2016.12.013
2. Konya CJ, Walter EJ (1991) Rock blasting and overbreak control. National Highway Institute. Federal Highway Administration Office of Implementation.
3. Singh TN, Singh V (2005) An intelligent approach to prediction and control ground vibration in mines. *Geotech Geol Eng* 23: 249–262. https://doi.org/10.1007/s10706-004-7068-x
4. Hajihassani M, Armaghani DJ, Sohaei H, et al. (2014) Prediction of airblast-overpressure induced by blasting using a hybrid artificial neural network and particle swarm optimization. *Appl Acoust* 80: 57–67. https://doi.org/10.1016/j.apacoust.2014.01.005
5. Jahed Armaghani D, Hajihassani M, Monjezi M, et al. (2015) Application of two intelligent systems in predicting environmental impacts of quarry blasting. *Arab J Geosci* 8: 9647–9665. https://doi.org/10.1007/s12517-015-1908-2

6. Sari M, Ghasemi E, Ataei M (2014) Stochastic modeling approach for the evaluation of backbreak due to blasting operations in open pit mines. *Rock Mech Rock Eng* 47: 771–783. https://doi.org/10.1007/s00603-013-0438-z
7. Zhou J, Li C, Koopialipoor M, et al. (2020) Development of a new methodology for estimating the amount of PPV in surface mines based on prediction and probabilistic models (GEP-MC). *Int J Min Reclam Environ* 35: 48–68. https://doi.org/10.1080/17480930.2020.1734151
8. Hosseini S, Monjezi M, Bakhtavar E, et al. (2021) Prediction of dust emission due to open pit mine blasting using a hybrid artificial neural network. *Nat Resour Res* 30: 4773–4788. https://doi.org/10.1007/s11053-021-09930-5
9. Hosseini S, Poormirzaee R, Hajihassani M, et al. (2022) An ANN-Fuzzy Cognitive Map-Based Z-Number Theory to Predict Flyrock Induced by Blasting in Open-Pit Mines. *Rock Mech Rock Eng* 55: 4373–4390. https://doi.org/10.1007/s00603-022-02866-z
10. Institute of Makers of Explosives, Glossary of commercial explosives industry terms. Institute of Makers of Explosive. Washington, 1997.
11. Raina AK, Murthy VMSR, Soni AK (2014) Flyrock in bench blasting: a comprehensive review. *Bull Eng Geol Environ* 73: 1199–1209. https://doi.org/10.1007/s10064-014-0588-6
12. Van der Walt J, Spiteri W (2023) A conceptual technique to mathematically quantify trajectory of flyrocks. *J S Afr Inst Min Metall* 123: 165–174. https://doi.org/10.17159/2411-9717/2168/2023
13. Verakis H, Lobb T (2007) Flyrock revisited: An ever-present danger in mine blasting. *Proceedings of the Annual Conference on Explosives and Blasting Technique* 33: 87–96.
14. Al-Bakri A, Hefni M (2021) A review of some non explosive alternative methods to conventional rock blasting. *Open Geosci* 13: 431–442. https://doi.org/10.1515/geo-2020-0245
15. Little TN (2007) Flyrock risk. *Proceedings of EXPLO Conference*, Wollongong, NSW, 35–43.
16. Szendrei T, Tose S (2022) Flyrock in surface mining- Limitations of current predictive models and better alternative through modelling the aerodynamics of flyrock trajectory. *J S Afr Inst Min Metall* 122: 725–732. https://doi.org/10.17159/2411-9717/1873/2022
17. Bhandari S (1997) Engineering rock blasting operations. A.A. Balkema, Rotterdam.
18. Richards AB, Moore JA (2005) Kalgoorlie consolidates gold mines: golden pieke cut-back flyrock control and calibration of a predictive model. Terrock Consulting Engineers.
19. Little TN, Blair DP (2010) Mechanistic Monte Carlo models for analysis of flyrock risk. In Rock Fragmentation by Blasting, *Rock Fragm Blasting* 9: 641–647.
20. Ghasemi E, Sari M, Ataei M (2012) Development of an empirical model for predicting the effects of controllable blasting parameters on flyrock distance in surface mines. *Int J Rock Mech Min Sci* 52: 163–170. https://doi.org/10.1016/j.ijrmms.2012.03.011
21. Szendrei T, Tose S (2023) Flyrock in surface mining Part II—Causes, sources, and mechanisms of rock projection. *J S Afr Inst Min Metall* 123: 557–564. https://doi.org/10.17159/2411-9717/2583/2023
22. Bright T, Amegbey N, Mireku-Gyimah D (2022) Prediction of flyrock throw using Gaussian process regression machine learning models. *ASRIC J Nat Sci* 1: 45–54.
23. Benin AK, Akuinor BT, Khandelwal M (2024) Estimating, appraising and establishing blast exclusion zone at Huni pit—A case study. *J Saf Sustain* 1: 98–107. https://doi.org/10.1016/j.jsasus.2024.01.001
24. Jenkins S, Floyd J (2000) Stemming enhancement tests. *Proceedings 26th Annual Conference on Explosives and Blasting Technique*, 2: 191–204.

25. Fletcher LR, D'Andrea DV (1986) Control of flyrock in blasting. *Proceedings 12th Annual Conference on Explosives and Blasting Technique*, 167–177.
26. Rehak TR, Bajpayee TS, Mowrey GL, (2001) Flyrock issues in blasting. *Proceedings 12th Annual Conference on Explosives and Blasting Technique*, 1: 165–175.
27. Bajpayee TS, Rehak TR, Mowrey GL, et al. (2002) A summary of fatal accidents due to flyrock and lack of blast area security in surface mining 1989–1999. *Proceedings 12th Annual Conference on Explosives and Blasting Technique.*
28. Verakis H, Lobb T (2003) An analysis of blasting accidents in mining operations. *Proceedings of the Annual Conference on Explosives and Blasting Technique*, 2: 119–130.
29. Kricak L, Kecojevic V, Negovanovic M, et al. (2012) Environmental and safety accidents related to blasting operation. *Am J Environ Sci* 8: 360–365.
30. Van der Walt J, Spiteri W (2020) A critical analysis of recent research into the prediction of flyrock and related issues resulting from surface blasting activities. *J S Afr Inst Min Metall* 120: 701–714. https://doi.org/10.17159/2411-9717/1103/2020
31. Dinh BT, Van TD, Van VP, et al. (2023) Simulation on flyrock due to blasting using smoothed particle hydrodynamics (SPH) with LS-Dyna software. *Inz Miner* 1: 13–22.
32. Bajpayee T, Verakis H, Lobb T (2004) An analysis and prevention of flyrock accidents in surface blasting operations. *Proceedings of the 30th Annual Conference on Explosives and Blasting Technique*, New Orleans, Louisiana, 2: 1–10.
33. Hustrulid WA (1999) Blasting principles for open pit mining: general design concepts. Balkema.
34. Olofsson SO (1990) Applied explosives technology for construction and mining. Sweden. Applex.
35. Blair DP (2022) Probabilistic analysis of flyrock from blasting in surface mines and quarries. *Int J Rock Mech Min Sci* 159: 105204. https://doi.org/10.1016/j.ijrmms.2022.105204
36. Ash RL (1963) The mechanics of rock breakage (part 2)—standards for blast design. Pit and Quarry, 118–122.
37. Ash RL (1977) Blasting Characteristics of Large Diameter Boreholes, *6th Annual Drilling and Blasting Technology*, Houston.
38. Bakhtavar E, Nourizadeh H, Sahebi AA (2017) Toward predicting blast-induced flyrock: a hybrid dimensional analysis fuzzy inference system. *Int J Environ Sci Technol* 14: 717–728. https://doi.org/10.1007/s13762-016-1192-z
39. Lundborg N (1974) The hazards of fly rock when blasting. Report DS 1974:12. Swedish Detonic Foundation (SveDeFo), Stockholm, Sweden.
40. Lundborg N, Persson A, Ladegaard-Pedersen A, et al. (1975) Keeping the lid on flyrock in open-pit blasting. *Eng Min J* 176: 95–100.
41. Monjezi M, Bahrami A, Varjani AY (2010) Simultaneous prediction of fragmentation and flyrock in blasting operation using artificial neural networks. *Int J Rock Mech Min Sci* 47: 476–480. https://doi.org/10.1016/j.ijrmms.2009.09.008
42. Rezaei M, Monjezi M, Varjani AY (2011) Development of a fuzzy model to predict flyrock in surface mining. *Saf Sci* 49: 298–305. https://doi.org/10.1016/j.ssci.2010.09.004
43. Khandelwal M, Monjezi M (2013) Prediction of flyrock in open pit blasting operation using machine learning method. *Int J Min Sci Technol* 23: 313–316. https://doi.org/10.1016/j.ijmst.2013.05.005

44. Yari M, Bagherpour R, Jamali S, et al. (2016) Development of a novel flyrock distance prediction model using BPNN for providing blasting operation safety. *Neural Comput Applic* 27: 699–706. https://doi.org/10.1007/s00521-015-1889-9
45. Jamei M, Hasanipanah M, Karbasi M, et al. (2021) Prediction of flyrock induced by mine blasting using a novel kernel-based extreme learning machine. *J Rock Mech Geotech Eng* 13: 1438–1451. https://doi.org/10.1016/j.jrmge.2021.07.007
46. Ding X, Jamei M, Hasanipanah M, et al. (2023) Optimized Data-Driven Models for Prediction of Flyrock due to Blasting in Surface Mines. *Sustainability* 15: 8424. https://doi.org/10.3390/su15108424
47. Faramarzi F, Mansouri H, Farsangi MAE (2014) Development of rock engineering systems-based models for flyrock risk analysis and prediction of flyrock distance in surface blasting. *Rock Mech Rock Eng* 47: 1291–1306. https://doi.org/10.1007/s00603-013-0460-1
48. Hasanipanah M, Jahed Armaghani D, Bakhshandeh Amnieh H, et al. (2018) A Risk-Based Technique to Analyze Flyrock Results Through Rock Engineering System. *Geotech Geol Eng* 36: 2247–2260. https://doi.org/10.1007/s10706-018-0459-1
49. Gupta RN (1990) Surface blasting and its impact on environment, *Impact of mining on environment*, Ashish Publishing House, New Delhi, 23–24.
50. Aghajani-Bazzazi A, Osanloo M, Azimi Y (2009) Flyrock prediction by multiple regression analysis in Esfordi phosphate mine of Iran. *Proceedings of the 9th International Symposium on Rock Fragmentation by Blasting*, 13–17, 649–657.
51. Supandi S (2024) New formula to determine flyrock distance on sedimentary rocks with low strength. *Open Geosci* 16: 20220624. https://doi.org/10.1515/geo-2022-0624
52. Richards AB, Moore AJ (2004) Flyrock control–By chance or design. *Proceedings 30th Annual Conference on Explosives and Blasting Technique*
53. Stojadinović S, Pantović R, Žikić M (2011) Prediction of flyrock trajectories for forensic applications using ballistic flight equations. *Int J Rock Mech Min Sci* 48: 1086–1094. https://doi.org/10.1016/j.ijrmms.2011.07.004
54. Raina AK, Murthy VMSR, Soni AK (2015) Estimating flyrock distance in bench blasting through blast induced pressure measurements in rock. *Int J Rock Mech Min Sci* 76: 209–216. https://doi.org/10.1016/j.ijrmms.2015.03.002
55. McKenzie C (2018) Flyrock model validation. *Proceedings of the ISEE Australia 4th Annual Conference*, Fremantle, WA. Available from: https://iseeaustralia.org/wp-content/uploads/2022/08/1_2McKenzie_FlyrockModelValidation-1.pdf.
56. Szendrei T, Tose S (2024) Flyrock in surface mining-Part 3: Shock wave, stress wave, blasthole expansion. *J S Afr Inst Min Metall* 124: 507–516. https://doi.org/10.17159/2411-9717/3321/2024
57. Stojadinović S, Lilić N, Pantović R, et al. (2013) A new model for determining flyrock drag coefficient. *Int J Rock Mech Min Sci* 62: 68–73. https://doi.org/10.1016/j.ijrmms.2013.04.002
58. Stojadinović, S, Lilić N, Obradović I, et al. (2015) Prediction of flyrock launch velocity using artificial neural networks. *Neural Comput Appl* 27: 515–524. https://doi.org/10.1007/s00521-015-1872-5
59. Raina AK, Murthy VMSR, Soni AK (2013) Relevance of shape of fragments on flyrock travel distance: An insight from concrete model experiments using ANN. *Electron J Geotech Eng* 18: 899–907.

60. Lemesh NI, Pozdnyakov BV (1972) The kinematics of motion of ledge rock in the zone of fracture during blasting. *Sov Min Sci* 8: 388–391. https://doi.org/10.1007/BF02497849
61. Roth J (1979) A model for the determination of flyrock range as a function of shot conditions. NTIS
62. Bagchi A, Gupta RN (1990) Surface blasting and its impact on environment. Workshop on Environmental Management of Mining Operations, Varanasi, 262–279.
63. Armaghani DJ, Mohamad ET, Hajihassani M, et al. (2016) Evaluation and prediction of flyrock resulting from blasting operations using empirical and computational methods. *Eng Comput* 32: 109–121. https://doi.org/10.1007/s00366-015-0402-5
64. Hasanipanah M, Faradonbeh RS, Armaghani DJ, et al. (2017) Development of a precise model for prediction of blast-induced flyrock using regression tree technique. *Environ Earth Sci* 76: 27. https://doi.org/10.1007/s12665-016-6335-5
65. Hudson JA (1992) *Rock Engineering Systems: Theory and Practice,* Ellis Horwood, Chichester.
66. Monjezi M, Mehrdanesh A, Malek A, et al. (2013) Evaluation of effect of blast design parameters on flyrock using artificial neural networks. *Neural Comput Applic* 23: 349–356. https://doi.org/10.1007/s00521-012-0917-2
67. Nguyen H, Tran BD, Bui NX, et al. (2025) Prediction of flyrock distance in open-pit mines using an optimized artificial neural network with evolution strategies. *J Min Earth Sci* 66: 15-28.
68. Trivedi R, Singh TN, Gupta N (2015) Prediction of Blast-Induced Flyrock in Opencast Mines Using ANN and ANFIS. *Geotech Geol Eng* 33: 875–891. https://doi.org/10.1007/s10706-015-9869-5
69. Hudaverdi T, Agan Y (2023) Application of Intelligent Models for Flyrock Prediction Considering Design Parameters and Bench Face Characteristics. *Min Metall Explor* 40: 2331–2347. https://doi.org/10.1007/s42461-023-00879-y
70. Ye J, He X (2023) A novel hybrid of ANFIS-based models using optimisation approaches to predict mine blast-induced flyrock. *Int J Environ Sci Technol* 20: 3673–3686. https://doi.org/10.1007/s13762-022-04170-3
71. Nguyen H, Van Thieu N (2025) Measurement and Prediction of Blast-Induced Flyrock Distance Using Unmanned Aerial Vehicles and Metaheuristic-Optimized ANFIS Neural Networks. *Nat Resour Res* 34: 1169–1198. https://doi.org/10.1007/s11053-024-10443-0
72. Nguyen H, Bao TD, Bui XN, et al. (2025) Measuring and Predicting Blast-Induced Flyrock Using Unmanned Aerial Vehicles and Lévy Flight Technique-Based Jaya Optimization Algorithm Integrated with Adaptive Neuro-Fuzzy Inference System. *Nat Resour Res* 34: 1773–1806. https://doi.org/10.1007/s11053-025-10455-4
73. Marto A, Hajihassani M, Armaghani DJ, et al. (2014) A novel approach for blast-induced flyrock prediction based on imperialist competitive algorithm and artificial neural network. *Sci World J* 2014: 643715. https://doi.org/10.1155/2014/643715
74. Wu M, Cai Q, Shang T (2019) Assessing the suitability of imperialist competitive algorithm for the predicting aims: an engineering case. *Eng Comput* 35: 627–636. https://doi.org/10.1007/s00366-018-0621-7
75. Amini H, Gholami R, Monjezi M, et al. (2012) Evaluation of flyrock phenomenon due to blasting operation by support vector machine. *Neural Comput Applic* 21: 2077–2085. https://doi.org/10.1007/s00521-011-0631-5
76. Rad HN, Hasanipanah M, Rezaei M, et al. (2018) Developing a least squares support vector machine for estimating the blast-induced flyrock. *Eng Comput* 34: 709–717. https://doi.org/10.1007/s00366-017-0568-0

77. Zhang R, Li Y, Gui Y, et al. (2024) A stacked multiple kernel support vector machine for blast induced flyrock prediction. *Geohazard Mech* 2: 37–48. https://doi.org/10.1016/j.ghm.2024.01.002
78. Hasanipanah M, Jahed Armaghani D, Bakhshandeh Amnieh H, et al. (2017) Application of PSO to develop a powerful equation for prediction of flyrock due to blasting. *Neural Comput Applic* 28: 1043–1050. https://doi.org/10.1007/s00521-016-2434-1
79. Zhou J, Koopialipoor M, Murlidhar BR, et al. (2019) Use of Intelligent Methods to Design Effective Pattern Parameters of Mine Blasting to Minimize Flyrock Distance. *Nat Resour Res* 29: 625–639. https://doi.org/10.1007/s11053-019-09519-z
80. Faradonbeh RS, Jahed Armaghani D, Monjezi M (2016) Development of a new model for predicting flyrock distance in quarry blasting: a genetic programming technique. *Bull Eng Geol Environ* 75: 993–1006. https://doi.org/10.1007/s10064-016-0872-8
81. Faradonbeh RS, Armaghani DJ, Monjezi M, et al. (2016) Genetic programming and gene expression programming for flyrock assessment due to mine blasting. *Int J Rock Mech Min Sci* 88: 254–264. https://doi.org/10.1016/j.ijrmms.2016.07.028
82. Dehghani H, Pourzafar M (2021) Prediction and minimization of blast-induced flyrock using gene expression programming and cuckoo optimization algorithm. *Environ Earth Sci* 80: 1–17.
83. Shamsi R, Amini M, Dehghani H, et al. (2022) Prediction of Fly-rock using Gene Expression Programming and Teaching– learning-based Optimization Algorithm. *J Min Environ* 13: 391–406.
84. Babaeian M, Sereshki F, Ataei M, et al. (2023) Application of Soft Computing, Statistical and Multi-Criteria Decision-Making Methods to Develop a Predictive Equation for Prediction of Flyrock Distance in Open-Pit Mining. *Mining* 3: 304–333. https://doi.org/10.3390/mining3020019
85. Saghatforoush A, Monjezi M, Shirani Faradonbeh R, et al. (2016) Combination of neural network and ant colony optimization algorithms for prediction and optimization of flyrock and back-break induced by blasting. *Eng Comput* 32: 255–266. https://doi.org/10.1007/s00366-015-0415-0
86. Zhou J, Lu Y, Tian Q, et al. (2024) Advanced Machine Learning Methods for Prediction of Blast-Induced Flyrock Using Hybrid SVR Methods. *Comput Model Eng Sci* 140: 1595–1617. https://doi.org/10.32604/cmes.2024.048398
87. Ding X, Hasanipanah M, Monjezi M, et al. (2025) Enhancing Mine Blasting Safety: Developing Intelligent Systems for Accurate Flyrock Prediction through Optimized Group Method of Data Handling Methods. *Nat Resour Res* 34: 1199–1218. https://doi.org/10.1007/s11053-024-10445-y
88. Faradonbeh RS, Armaghani DJ, Amnieh HB, et al. (2018) Prediction and minimization of blast-induced flyrock using gene expression programming and firefly algorithm. *Neural Comput Applic* 29: 269–281. https://doi.org/10.1007/s00521-016-2537-8
89. Asl PF, Monjezi M, Hamidi JK, et al. (2018) Optimization of flyrock and rock fragmentation in the Tajareh limestone mine using metaheuristics method of firefly algorithm. *Eng Comput* 34: 241–251. https://doi.org/10.1007/s00366-017-0535-9
90. Li D, Koopialipoor M, Armaghani DJ (2021) A Combination of Fuzzy Delphi Method and ANN-based Models to Investigate Factors of Flyrock Induced by Mine Blasting. *Nat Resour Res* 30: 1905–1924. https://doi.org/10.1007/s11053-020-09794-1
91. Murlidhar BR, Nguyen H, Rostami J, et al. (2021) Prediction of flyrock distance induced by mine blasting using a novel Harris Hawks optimization-based multi-layer perceptron neural network. *J Rock Mech Geotech Eng* 13: 1413–1427. https://doi.org/10.1016/j.jrmge.2021.08.005

92. Li C, Zhou J, Du K, et al. (2023) Prediction of Flyrock Distance in Surface Mining Using a Novel Hybrid Model of Harris Hawks Optimization with Multi-strategies-based Support Vector Regression. *Nat Resour Res* 32: 2995–3023. https://doi.org/10.1007/s11053-023-10259-4
93. McKenzie C (2008) Rango de Flyrock and Predicción del Tamaño de los Fragmentos. Conferencia ASIEX. Pucón.
94. Trivedi R, Singh TN, Raina AK (2014) Prediction of blast-induced flyrock in Indian limestone mines using neural networks. *J Rock Mech Geotech Eng* 6: 447–454. https://doi.org/10.1016/j.jrmge.2014.07.003
95. Davies PA (1995) Risk-based approach to setting of flyrock danger zones for blast sites. *Int J Rock Mech Min Sci Geomech Abstr* 6: 278A.
96. St George JD, Gibson MFL (2001) Estimation of flyrock travel distances: a probabilistic approach. *Proceedings Explo*, 28–31.
97. Raina AK, Chakraborty AK, Choudhury PB, et al. (2011) Flyrock danger zone demarcation in opencast mines: a risk based approach. *Bull Eng Geol Environ* 70: 163–172. https://doi.org/10.1007/s10064-010-0298-7
98. Chernigovskiĭ AA (1985) *Application of directional blasting in mining and civil engineering*. Oxonian Press.
99. Feng CC, Wang ZL, Wang JG, et al. (2024) A thermos-mechanical damage constitutive model for deep rock considering brittleness-ductility transition characteristics. *J Cent South Univ* 31: 2379–2392. https://doi.org/10.1007/s11771-024-5700-x
100. Wang Z, Wang H, Wang J, et al. (2021) Finite element analyses of constitutive models performance in the simulation of blast-induced rock cracks. *Comput Geotech* 135: 104172. https://doi.org/10.1016/j.compgeo.2021.104172
101. Wang ZL, Li YC, Shen RF (2007) Numerical simulation of tensile damage and blast crater in brittle rock due to underground explosion. *Int J Rock Mech Min Sci* 44: 730–738. https://doi.org/10.1016/j.ijrmms.2006.11.004
102. Hustrulid W, Johnson J (2008) A gas pressure-based drift round blast design methodology. *5th International Conference and Exhibition on Mass Mining*, Lulea University of Technology, 657–669.
103. Chiappetta RF, Mammele ME (1988) Use of high-speed motion picture photography in blast evaluation and design, *High Speed Photography, Videography, and Photonics*, 319–336. https://doi.org/10.1117/12.942247

AIMS Press